Cerium oxide nanoparticles modulate liver X receptor and short heterodimer partner, and attenuate liver steatosis and steatohepatitis in a rat model of postmenopausal obesity

Fatma M. Lebda[1], Sahar M. El Agaty[1] , Radwa H. Ali[1,2], Ghada Galal Hamam[3], Aliaa M. Abd El-Monem[1] and Noha N. Lasheen[1,4]

[1] *Department of Physiology, Faculty of Medicine, Ain Shams University, Cairo, Egypt*
[2] *Department of Physiology, Faculty of Medicine, Armed Forces College of Medicine (AFCM), Cairo, Egypt*
[3] *Department of Histology, Faculty of Medicine, Ain Shams University, Cairo, Egypt*
[4] *Department of Physiology, Faculty of Medicine, Galala University, Suez, Egypt*

Abstract. This study aimed to investigate the effect of cerium oxide nanoparticles (CeO_2-NPs) on non-alcoholic fatty liver disease in postmenopausal obesity and the underlying mechanisms.64 adult female rats were allocated into Sham, ovariectomized (OVX), high-fat high-fructose diet-fed-OVX (HFHF-OVX), and HFHF-OVX-CeO_2-NPs-treated (CeO_2-HFHF-OVX) groups. OVX and HFHF-OVX rats presented a significant increase in overall and visceral obesity, dyslipidemia, liver enzymes, serum malondialdehyde, liver TNF-α, TGF-β1 and free fatty acids, liver X receptor (LXR) expression associated with decreased serum total antioxidant capacity and liver short heterodimer partner (SHP) expression *vs.* Sham group. Also, histomorphometric studies displayed a significant higher scores of liver steatosis, inflammation and fibrosis. All these parameters were significantly improved by CeO_2-NPs treatment in CeO_2-HFHF-OVX *vs.* HFHF-OVX rats. Thus, CeO_2-NPs treatment ameliorates liver steatosis, steatohepatitis, and fibrosis in postmenopausal obese rats *via* alleviation of obesity, dyslipidemia, modulating liver genes involved in lipid metabolism (LXR and SHP), decreasing liver lipogenesis besides its antioxidant and anti-inflammatory effects.

Key words: Cerium — Liver X receptors — Nanoparticles — Non-alcoholic fatty liver disease — Obesity — Postmenopause

Introduction

Non-alcoholic fatty liver disease (NAFLD) is characterized by excessive hepatic lipid accumulation which is not related to alcohol use. It involves many hepatic pathologies that range from isolated hepatic steatosis, non-alcoholic steatohepatitis (NASH), up to liver fibrosis, and cirrhosis (Chalasani et al. 2018). The pathogenesis of NAFLD begins with an initial stage of hypertriglyceridemia with disturbed hepatic lipid metabolism followed by second stage of inflammation and oxidative stress which ultimately lead to NASH (Manne et al. 2018). Progressive withdrawal of estrogen is associated with many risks that signal the development and progression of NAFLD/NASH in menopause. Obesity and dyslipidemia are triggered by estrogen loss and primarily drive the process of liver lipid infiltration (Palmisano et al. 2017). Moreover, earlier reports have postulated a regulatory effect of estrogen on genes of lipid metabolism pathways in the liver such as liver tissue X receptor (LXR) and short heterodimer partner (SHP) (Han et al. 2014; Wang et al. 2015).

Correspondence to: Sahar M. El Agaty, Department of Physiology, Faculty of Medicine, Ain Shams University, Abasia, Cairo, Egypt
E-mail: sahar_elagaty@ yahoo.com; saharelagaty@med.asu.edu.eg

Although, hormone replacement therapy provides a hepatoprotective effect on the development of NAFLD in menopausal women, it is not a convenient line of treatment because it has been linked to detrimental diseases such as thromboembolism, breast cancer and ovarian cancer (Lobo 2017). Therefore, a safe therapy that can decrease metabolic derangement, oxidative stress and inflammation may help in prevention of the development or the acceleration of NAFLD in menopause. Cerium oxide nanoparticles (CeO_2-NPs) or nanoceria, have shown promising approaches as therapeutic agents in biology and medical sciences (Charbgoo et al. 2017). CeO_2-NPs, a rare earth metal oxide, had proven to behave as free radical scavengers, and anti-inflammatory agents (Hirst et al. 2009), and displayed potent catalase- and super oxide dismutase-mimetic (SOD) activity (DeCoteau et al. 2016; Tian et al. 2017). Recent studies demonstrated that CeO_2 has advantage over classic antioxidants such as SOD, ascorbic acid, resveratrol, colchicine, eugenol, and vitamin E (Casals et al. 2021). CeO_2-NPs act as scavenger system against different reactive oxygen species (ROS) and reactive nitrogen species (Charbgoo et al. 2017); and have a self regenerating mechanism (Casals et al. 2020). Experimental studies demonstrated that nanoceria is effective against hepatic ischemia reperfusion injury by reducing ROS level and inhibiting the inflammatory cascades (Manne et al. 2017; Ni et al. 2019) and exerts hepatoprotective activity in a rat model of liver fibrosis induced by CCl_4 (Oró et al. 2016). In addition, CeO_2-NPs enhance liver regeneration in experimental models of acetaminophen-induced liver toxicity and partial hepatectomy (Córdoba-Jover et al. 2019).

In this context, this study was designed to determine whether CeO_2-NPs display hepatoprotective properties against experimentally induced NAFLD in a rat model of postmenopausal obesity and to explore the underlying mechanism of action. An experimental model of postmenopausal obesity was produced in the present study by bilateral ovariectomy in rats, a well-established animal model that mimics menopausal changes (Khajuria et al. 2012), and by feeding high-fat, high-fructose diet (HFHF) to rats after the surgery.

Materials and Methods

Animals

Sixty-four female Wistar rats, weighing 200–250 g were obtained from Helwan farm, Cairo, Egypt. Rats were maintained under regular 12 h:12 h light/dark cycle and standard conditions of boarding with room temperature 22–25°C in Medical Ain Shams Research Institute (MASRI), Faculty of Medicine, Ain Shams University. Rats were acclimated for 7 days before the start of the experiment. All the experimental procedures were conducted according to National Institutes of Health Guide for the Care and Use of Laboratory Animal, and the study protocol was approved by the Research Ethical Committee of Faculty of Medicine, Ain Shams University (FMASU, MD 362/2018). The "Principles of laboratory animal care" (NIH publication No. 86-23, revised 1985) were followed, as well as specific national laws.

The ovariectomy operation

It was performed according to the method described by Khajuria et al. (2012). After anaesthesia (80 mg/kg ketamine), a single lower abdominal incision was made above the symphysis pubis. The ovary was exposed on each side, and haemostasis was insured by ligation of the upper horns of the uterus with a chromic catgut thread. Each ovary, together with its surrounding fat and oviduct, was removed. Then, the wound was closed. Asepsis and analgesia were maintained by ceftriaxone (40 mg/kg i.m.) and diclofenac potassium (5 mg/kg, i.m.) for 48 h postoperatively. The sham-operated rats were treated in a similar way, but only the ovaries and oviduct were manipulated. After full recovery (10 days after the operation), the experiment started and extended for 8 weeks.

Preparation of dietary formula

The HFHF diet formula (35.5% fat, 32.4% carbohydrate (CHO) and 18% proteins, in 100 g of dry food with a total caloric value of 521 kcal/100 g dry food), and the normal chow diet formula (7.2% fats, 60% CHO and 18.2% proteins, in 100 g of dry food, with a total caloric value of 377.5 kcal/100 g dry food) were prepared according to Feillet-Coudray et al. (2019), and administered to rats for 8 weeks.

CeO^2-NPs treatment

CeO_2-NPs (Sigma-Aldrich, St. Louis, MO, USA, code 544841) were freshly dissolved in 0.5 ml of sterile phosphate-buffered saline (PBS, pH 7.4) and mixed for 5 min, before administration, using Thermolyne 37600 mixer (Barnstead, USA). CeO_2-NPs were intraperitoneally (i.p.) injected, in a dose 0.1 mg/kg, twice/week for the first two weeks of the experiment (Nassar et al. 2018).

Characterization of CeO^2-NPs

This was done at Electron Microscopy Unit, Faculty of Medicine for Males, Al Azhar University, using an electron microscope (Jeo 100C, Tokyo, Japan).

The suspension of cerium oxide was characterized by using transmission electron microscopy (TEM). A small drop of the suspension was placed onto TEM grids coated with a thin carbon film and allowed to evaporate. Then, digital pictures of several locations on the grid were taken. TEM examination of cerium oxide nanoparticles suspension appeared as particles within a range of 10–25 nm in size measured by TEM scale. They were spherical to cuboidal in shape, electron dense and formed aggregates of different sizes (Fig. 1).

Experimental design

Rats were randomly allocated into four groups. 1) Sham-operated group (Sham, n = 17), rats in this group were subjected to sham operation (all steps of ovariectomy operation, without removal of the ovaries), then, they were fed normal chow diet for 8 weeks. 2) Ovariectomized group (OVX, n = 16); rats in this group were subjected to bilateral ovariectomy, thereafter they were fed normal chow diet for 8 weeks. 3) High-fat high-fructose diet-fed ovariectomized group (HFHF-OVX, n = 15), rats in this group were subjected to bilateral ovariectomy, then, they were fed HFHF diet for 8 weeks. 4) HFHF diet-fed ovariectomized, CeO$_2$-NPs-treated group (CeO$_2$-HFHF-OVX, n = 16), rats in this group were subjected to bilateral ovariectomy, then, they were fed HFHF diet for 8 weeks, and i.p. injected by cerium oxide nanoparticles in a dose 0.1 mg/kg, twice/week for the first 2 weeks of the experimental period.

Experimental procedure

On the day of sacrifice, overnight fasted rats were weighed and anaesthetized by i.p. injection of pentobarbitone, in a dose of 40 mg/kg. Then, the length of the rat was measured from the tip of the nose to the anus and used to calculate body mass index (BMI) according to the following equation: BMI = body weight (BW, g)/length^2 (cm^2). Also, the waist circumference (WC) was measured. Then a midline abdomi-

nal incision was made, the abdominal aorta was exposed and cannulated with a polyethylene catheter, and blood samples were collected in two serum clot activator plastic tubes with gel. The tubes were centrifuged at 4000 rpm for 15 min and the supernatant serum was stored at –80°C until used for determination of liver enzymes, alanine amino transferase (ALT) and aspartate aminotransferase (AST); lipid profile, triglycerides (TG), total cholesterol (TC), and high-density lipoprotein cholesterol (HDL-C); and oxidative stress markers, malondialdehyde (MDA), and total antioxidant capacity (TAC). All biochemical analysis was conducted blindly by an expert clinical pathologist. Then, visceral fat was excised, washed, dried by filter paper and weighed in 5-Digit-Metler balance (Sartorious AG, bl-210s). The visceral fat weight (VFW) results were expressed as absolute values (g) and relative values to the body weight (VFW/BW, g/g). The liver was excised, and the left lobe was used for histopathological studies and the right lobe was stored at –80°C for later determination of free fatty acid (FFA), tumor necrosis factor-alpha (TNF-α), transforming growth factor-beta1 (TGF-β1), gene expression of SHP and LXR.

Biochemical analysis

Measurement of liver enzymes

Serum ALT and AST activities were measured by using colorimetric kits supplied by Egy-Chem. for lab. technology, Egypt (ALT, CAT. No. GPT113240; AST, CAT. No. GOT110240).

Measurement of lipid profile

Serum levels of TGs, TC, and HDL-C were determined by enzymatic colorimetric method by using colorimetric kits supplied by Biodiagnostic, Egypt (TGs, CAT. No. TR 20 30; TC, CAT. No. CH 12 20; HDL-C, CAT. No. CH 12 30). Low-density lipoprotein cholesterol (LDL-C, mg/dl) was calculated according to Friedewald et al. (1972) using the
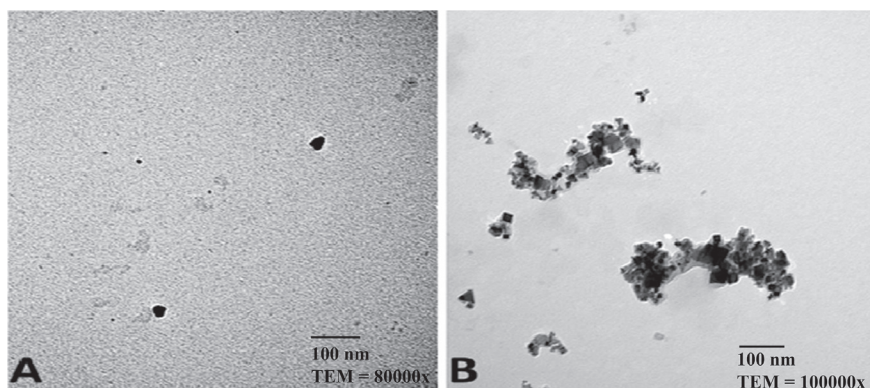

Figure 1. The representative electron micrograph of cerium oxide nanoparticles (**A**) and aggregates of cerium oxide nanoparticles of different sizes (**B**) in suspension.

following equation: LDL-C = TC – (HDL-C + TG/S). Atherogenic index (AI) was calculated according to Onat et al. (2010) as follows: $AI = \log_{10}TG/HDL\text{-}C$.

Measurement of oxidative stress markers

Serum levels of MDA and TAC were determined by using colorimetric kits supplied by Biodiagnostic, Egypt (MDA, CAT. No. 25 28; TAC, CAT. NO. TA 25 12).

Measurement of liver tissue levels of TNF-α, TGF-β1, and FFA

Liver tissue TNF-α was measured by using Rat TNF-alpha ELISA Kit supplied by RayBiotech (Inc., Norcross, Georgia, USA, CAT. No. ELR-TNFa), TGF-β1 was measured by using Rat TGF-β1 PicoKine ELISA Kits (Pleasanton, USA, CAT. No. MBS824788). The level of FFA in liver tissue was determined by using Rat FFA ELISA Kit (BioSource International, Inc., California, USA, Cat. No: MBS014345).

Gene expression of short heterodimer partner and LXR Real-time quantitative PCR (qPCR) analysis

RNA extraction and cDNA conversion

Total RNA was isolated using Qiagen tissue extraction kit (Qiagen, USA, CAT. No. 51304) according to the instructions of manufacture. The purity (A260/A280 ratio) and the concentration of RNA were obtained using spectrophotometry (dual wavelength Beckman, Spectrophotometer, USA). A cDNA synthesis reaction was performed using the reverse transcription kit (Fermentas, USA). 3 μl of random primers were added to 10 μl of RNA, which was denatured for 5 min at 65°C in the thermal cycler. The RNA primer mixture was cooled to 4°C, and the cDNA master mix was prepared according to the kit instructions. Total volume of the master mix was 19 μl for each sample. This was added to the 31 μl of RNA-primer mixture resulting in 50 μl of cDNA. The last mixture was incubated in the programmed thermal cycler one hour at 37°C followed by inactivation of enzymes at 95°C for 10 min, and finally cooled at 4°C, then, RNA was changed into cDNA. The converted cDNA was stored at –20°C.

Real-time qPCR

Real-time qPCR amplification and analysis were performed using an Applied Biosystem with software version 3.1 (StepOne™, USA). The Real-time qPCR assay with the primer sets were optimized at the annealing temperature. Amplification of the synthesized cDNA was performed in duplicates for each gene and endogenous reference control (β actin). Every reaction had a total volume of 25 μl con-

taining 12.5 μl Syber green mix, 1 μl Forward primer, 1 μl Reverse primer, 5 μl cDNA template and 5.5 μl RNAse free water. The real-time cycler consisted of one cycle at 50°C for 2 min followed by 40 cycles of denaturation at 95°C for 15 s, 1 min at 60°C for annealing, and 1 min at 72°C for extension.

Relative expression of studied genes was calculated using Applied Biosystem software. All values were normalized to β actin levels as a reference gene. The primer pair sequence used for each gene are listed as follows: SHP (Forward primer; 5'-AGTTGGAAAGTTGGAGTG-3'; Reverse primer: 5'-GATTGTTGTATGGGGAGTA-3'); LXR (Forward primer: 5'-CTGATTCTCCGTGTCCTCTGTG-3'; Reverse primer : 5'-CACCCTACCCTTTGACTCTCT-3'); β actin (Forward primer: 5'-CCC ATC TAT GAG GGT TAC GC-3'; Reverse primer : 5'-TTT AAT GTC ACG CAC GAT TTC-3').

Histopathological studies

The liver specimens were collected and fixed in 10% formalin and embedded in paraffin. Six micrometer sections were cut, deparaffinized, hydrated and stained with Hematoxylin and Eosin (H&E). To determine liver fibrosis paraffin sections were stained with Masson's trichrome stain which reveals collagen fibers deposition in green color. Localization of fat droplets was determined in ten micrometer frozen liver sections (−80°C), by using Oil Red O stain.

Histomorphometric studies that determine the mean area percentage of collagen fibers in Masson`s trichrome stained section, and the mean area percentage of fat droplets in Oil Red O stained sections were measured using, Leica DM2500 microscope, with a Canon EOS 1100D Digital SLR camera, and image analyzer Leica Q win V.3 program installed on a computer connected to a Leica DM2500 microscope (Wetzlar, Germany).

For quantified evaluation of tissue changes, all liver specimens were reviewed and scored according to Non-alcoholic Steatohepatitis Clinical Research Network (Brunt et al. 1999; Kleiner et al. 2005; Tandra et al. 2011). Liver specimens from five different rats from each group were subjected to morphometric study. Four different haphazardly selected, non-overlapping fields were photographed to be examined. So, for each parameter 20 different microscopic fields were obtained. The number and frequency distribution (%) of each examined component was calculated as a percentage form 20 (four different field sections in five rats (20 fields/group)). H&E staining was used to evaluate all features except fibrosis. Masson's trichrome staining was used for evaluation of fibrosis only.

Diagnosis and grading of NAFLD, NASH and liver fibrosis were as follows: Steatosis (Macrovesicular steatosis), 0 = < 5% liver cells involved, 1 = 5–33% liver cells involved, 2 = 34–66% liver cells involved, and 3 = > 66% liver cells

involved; Lobular and portal inflammation, 0 = none, 1 = 1–2 foci, 2 = up to 4 foci, and 3 = > 4 foci; Hepatocellular ballooning, 0 = absent, 1 = few cells in some lobules, 2 = few cells in most lobules, and 3 = many cells of most lobules; Presence of Mallory-Denk bodies, 0 absent, 1 is occasional and 2 is several; Lobular fibrosis, 0 absent, 1 = Zone 3 or periportal, 2 = Zone 3 and periportal, 3 = bridging fibrosis with architectural distortion, and 4 = cirrhosis; and Portal fibrosis was scored from 0–4; 0 absent, 1 = enlarged, fibrotic portal tracts, 2 = periportal or portal-portal septa with intact architecture, 3 = bridging fibrosis, and 4 = cirrhosis. In each group, five liver sections were prepared from five randomly selected rats. Then, four different non-overlapping fields were examined from each section. Thus, 20 fields were used for measuring every morphometric parameter in the individual group.

Statistical analysis

Biochemical variables were presented as mean ± standard error of mean (SEM). The one-sample Kolmogorov-Smirnov test was used to assess normality of variables and all variables were normally distributed. One way ANOVA was done to determine the differences between groups and in case of significant 'F' test ($p \leq 0.05$), *post-hoc* test was made by Fisher's least significant difference to find inter-group significance. Data of the histological damage scores were presented as median and range, and the statistical analysis was determined using Kruskal-Wallis test followed by the Mann-Whitney U-test. Spearman correlation analysis was used to investigate the relationship between LXR and SHP, and liver FFA, lipid profile as well as histological scores. A value of $p \leq 0.05$ was considered statistically significant.

Results

Changes in anthropometric parameters

The BW and the BMI as well as their percent change were significantly increased in OVX rats *vs.* Sham group; and in HFHF-OVX rats *vs.* Sham and OVX groups (Fig. 2). Also, WC, VFW, and relative VFW were significantly increased in OVX and OVX-HFHF rats compared to Sham group. CeO$_2$-NPs treatment significantly decreased all these parameters in CeO$_2$-HFHF-OVX rats *vs.* both OVX and HFHF-OVX groups; all approached the sham values except the % change of BW and WC.

Changes in liver enzymes

As shown in Figure 3, serum AST and ALT were significantly increased in OVX rats *vs.* Sham group; and in HFHF-OVX rats *vs.* Sham and OVX groups. CeO$_2$-NPs treatment significantly decreased both enzymes in CeO$_2$-HFHF-OVX rats *vs.* HFHF-OVX group, though they were still significantly higher than their matched values in Sham group.

Changes in the mRNA expression of LXR and SHP in liver and FFA liver levels

Liver LXR expression and FFA levels showed a significant increase associated with a significant decrease in liver SHP expression in OVX rats *vs.* Sham group; and in HFHF-OVX rats *vs.* Sham and OVX groups (Fig. 3). CeO$_2$-NPs treatment resulted in a significant decrease in liver LXR expression and FFA levels along with a significant increase in liver SHP expression in CeO$_2$-HFHF-OVX rats compared to OVX and HFHF-OVX groups, however, all parameters did not approach the sham values.

Changes in lipid profile and atherogenic index

Serum levels of TG, TC, LDL-C and AI were significantly increased, associated with a significant decrease in HDL-C in OVX rats compared to Sham group; and in HFHF-OVX rats compared to sham and OVX groups (Table 1). Treating HFHF-OVX rats with CeO$_2$-NPs significantly diminished serum levels of TG, TC, LDL-C and AI, and significantly elevated HDL-C in CeO$_2$-HFHF-OVX rats compared to both OVX and HFHF-OVX groups, however, all parameters did not reach the sham values.

Changes in oxidative stress and inflammatory markers

As demonstrated in Table 1, serum MDA, liver tissue TNF-α, and liver tissue TGF-β1, were significantly increased along with a significantly decreased serum TAC in OVX rats compared to Sham group; and in HFHF-OVX rats compared to Sham and OVX groups. Meanwhile, CeO$_2$-HFHF-OVX group showed a significantly decreased serum MDA, liver tissue TNF-α, and liver tissue TGF-β1 accompanied by a significantly increased TAC compared to both OVX and HFHF-OVX groups, although all markers did not achieve the sham values.

Correlation studies

As shown in Table 2, LXR expression was significantly and positively correlated with liver enzymes, liver FFA, TG, TC, LDL-C, as well as histological scores of liver steatosis, liver inflammation, Mallory Bodies, and ballooning. On the contrary, all these parameters were significantly and negatively correlated with SHP expression. Also, HDL-C showed a significant and negative relationship with LXR, and a significant and positive relationship with SHP.

Histological results

H&E-stain

Sham group showed the general appearance of classic hepatic lobules. Central veins were present in the middle of hepatic lobules, and portal tracts were observed at the periphery (Fig. 4A). Cords of hepatocytes were seen radiating from the central vein in branching and anastomosing pattern. Hepatocytes were polygonal in shape with acidophilic cytoplasm and central rounded vesicular nuclei. Some hepatocytes were binucleated. Blood sinusoids were noticed as slit-like spaces between hepatocytes and were lined with flat endothelial cells (Fig. 4B). Portal areas were seen containing bile ducts, branches from hepatic artery and portal vein (Fig. 4C).

OVX group showed mononuclear cellular infiltrations in most portal tracts (Fig. 4D). Hepatic sinusoids were sometimes observed dilated (Fig. 4E). Accumulation of inflammatory cells were, also, seen between hepatocytes (Fig. 4E and F) and in the portal tracts (Fig. 4G). Mal-
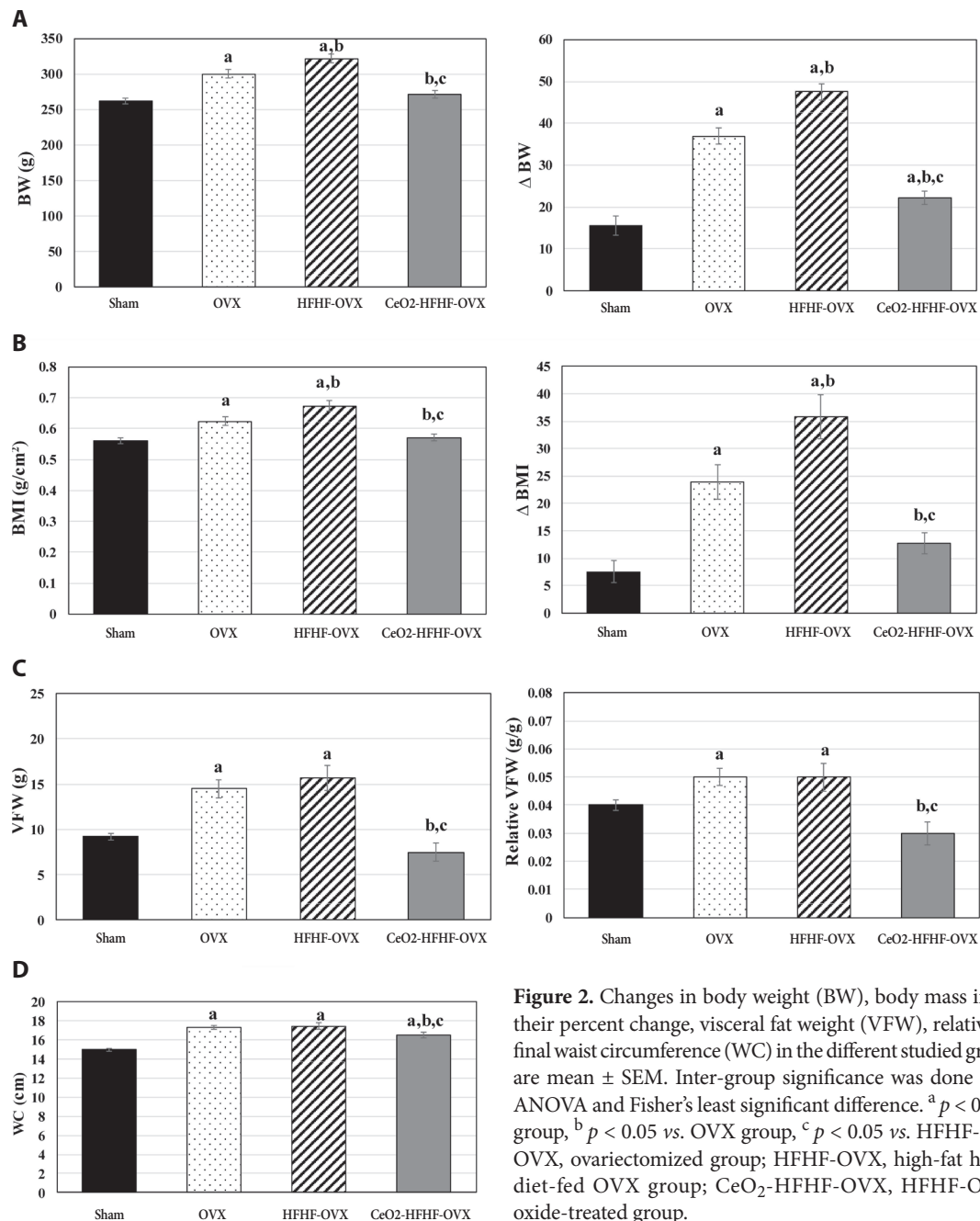

Figure 2. Changes in body weight (BW), body mass index (BMI), their percent change, visceral fat weight (VFW), relative VFW and final waist circumference (WC) in the different studied groups. Values are mean ± SEM. Inter-group significance was done by One way ANOVA and Fisher's least significant difference. [a] $p < 0.05$ vs. Sham group, [b] $p < 0.05$ vs. OVX group, [c] $p < 0.05$ vs. HFHF-OVX group. OVX, ovariectomized group; HFHF-OVX, high-fat high-fructose diet-fed OVX group; CeO$_2$-HFHF-OVX, HFHF-OVX cerium oxide-treated group.
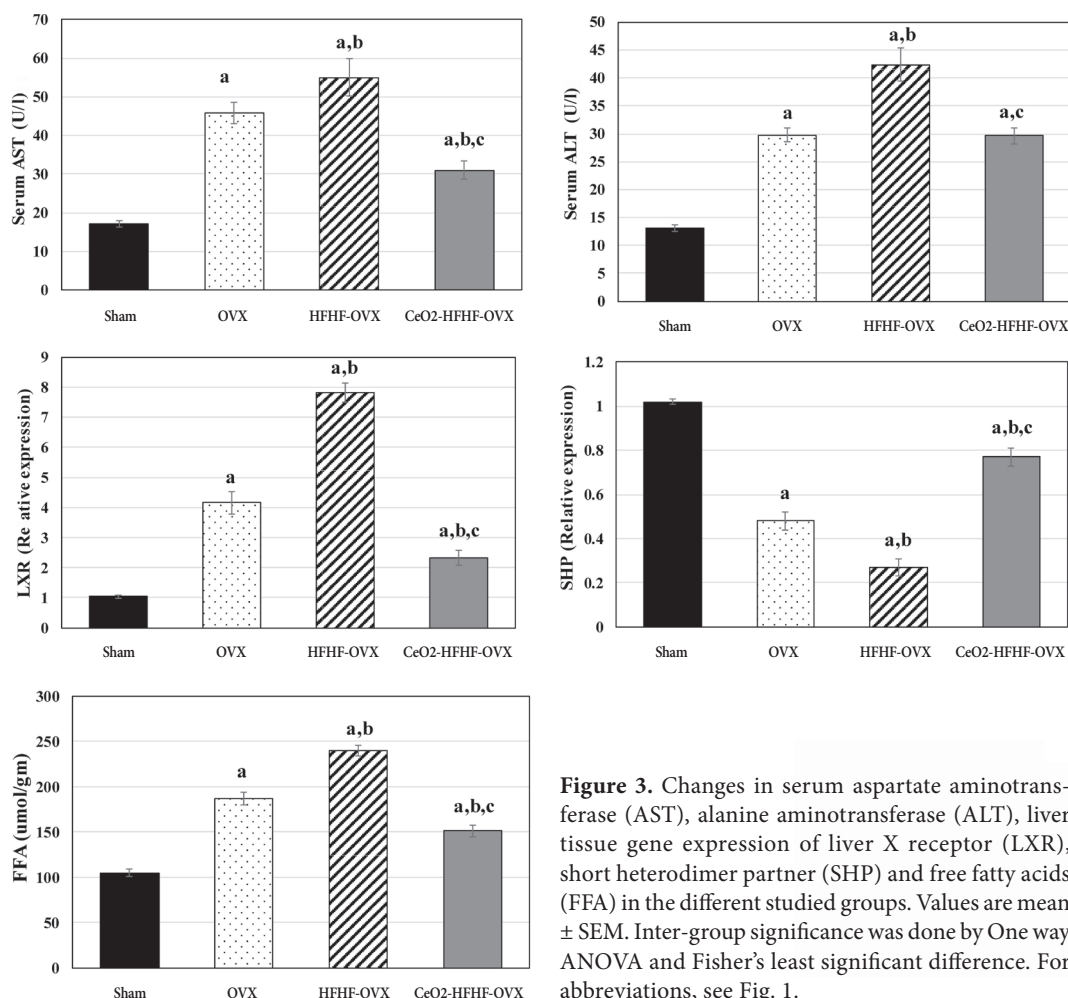
Figure 3. Changes in serum aspartate aminotransferase (AST), alanine aminotransferase (ALT), liver tissue gene expression of liver X receptor (LXR), short heterodimer partner (SHP) and free fatty acids (FFA) in the different studied groups. Values are mean ± SEM. Inter-group significance was done by One way ANOVA and Fisher's least significant difference. For abbreviations, see Fig. 1.

lory bodies were noticed inside some hepatocytes, which appeared as deep eosinophilic intracytoplasmic structure (Fig. 4F).

Intracellular vacuoles were present in the cytoplasm of hepatocytes near the portal tracts (Fig. 4G). Some portal tracts were expanded with dilated congested portal vein branches and dilated proliferated bile ducts (Fig. 4H).

In HFHF-OVX group, expanded portal tracts and bridging between portal tracts of adjacent lobules were frequently noted (Fig. 5A). Inflammatory cells were present in most portal tracts (Fig. 5A and B). Hepatocytes in most lobules had vacuolated cytoplasm and deeply stained nuclei (Fig, 5B). Some of these nuclei were pushed peripherally. Disturbed radial arrangement of hepatic cords and obliterated blood sinusoids were, also, frequently noted. In addition, ballooned hepatocytes with shrunken deeply stained pyknotic nuclei and Mallory bodies were frequently noticed. Mallory bodies were eosinophilic structure and was seen inside most hepatocytes (Fig. 5C). Dilated congested hepatic sinusoids were, also, present (Fig. 5D), in addition to expanded portal tracts with inflammatory cells (Fig. 5E and F) and proliferations of bile ducts were frequently observed (Fig. 5F).

CeO$_2$-HFHF-OVX group showed normal hepatic architecture in most hepatic lobules. Focal areas of vacuolated hepatocytes were sometimes noticed (Fig. 6A). Few dilated congested hepatic sinusoids were occasionally seen (Fig. 6B). Some hepatocytes had intracellular vacuoles and peripheral nuclei (Fig. 6B and C). Other hepatocytes were ballooned (Fig. 6C). Few inflammatory cells were present in some portal tracts (Fig. 6D).

Masson`s trichrome stain

Sham rats showed few collagen fibers around central veins, portal tracts and between hepatocytes (Fig. 7A). OVX group demonstrated increase amounts of collagen fibers in some portal tracts and in-between hepatocytes (Fig. 7B). HFHF-OVX group showed increased amounts of collagen fibers in the expanded portal tracts and in-
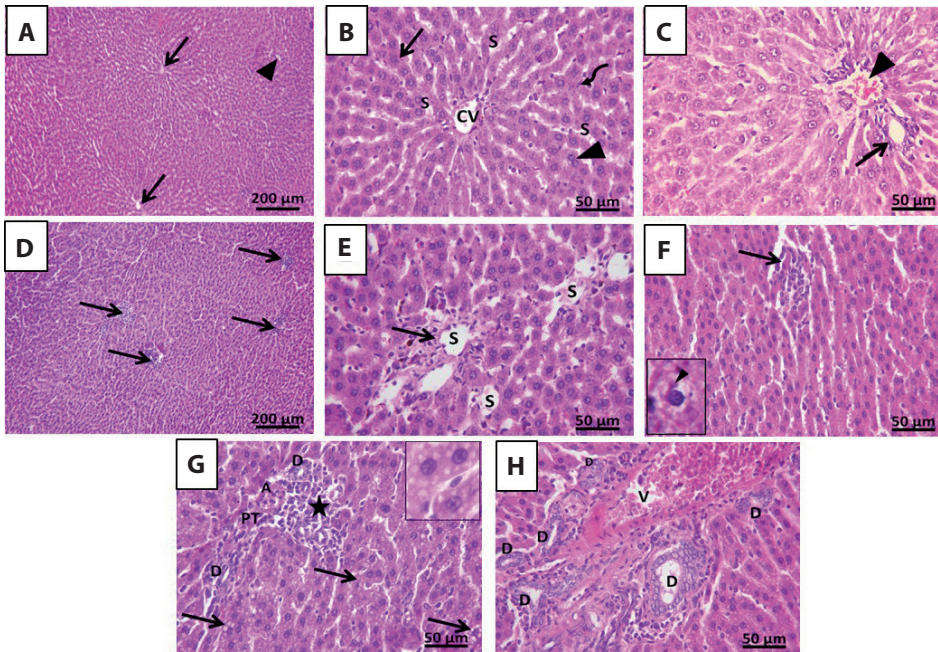
Figure 4. Photomicrographs of H&E stained liver sections from Sham (A–C) and OVX (D–H) groups. **A.** The general appearance of classic hepatic lobules. Central vein (↑) is seen in the middle of the lobule and portal tracts (▲) are seen at the periphery (×100). **B.** Cords of hepatocytes radiation from the central vein (CV) in branching and anastomosing pattern. Hepatocytes are polygonal in shape with acidophilic cytoplasm and central rounded vesicular nuclei (↑). Some hepatocytes are seen binucleated (▲). Blood sinusoids (S) are slit like spaces between hepatocytes and are lined with flat endothelial cells (curved arrow) (×400). **C.** The portal area containing branches from bile duct (↑), hepatic artery and portal vein (▲) (×400). **D.** Foci of inflammatory cellular infiltrations (↑) in the portal tracts (×100). **E.** Areas of dilated hepatic sinusoids (S). Inflammatory cells (↑) are also seen between hepatocytes (×400). **F.** Accumulation of inflammatory cells (↑) between hepatocytes in the middle of hepatic lobule. Inset: Mallory body (▲) is seen inside hepatocyte as deep eosinophilic structure (×400, inset ×1000). **G.** Portal tract (PT) containing bile duct branches (D) and accumulation of inflammatory cells (*). Hepatocytes with intracellular vacuoles (↑) are seen. Inset: intracellular vacuoles in the cytoplasm of hepatocytes (×400, inset ×1000). **H.** Expanded portal tract with dilated congested portal vein branch (V) and proliferation of bile ducts (D) (×400). For abbreviations, see Fig. 1.

between hepatocytes (Fig. 7C). On the other hand, CeO$_2$-HFHF-OVX group showed minimal amounts of collagen fibers around central veins, portal tracts and in-between hepatocytes (Fig. 7D).

Oil Red O stain

Examination of frozen sections stained with Oil Red O stain showed no red deposits of lipid droplets in hepatocytes of
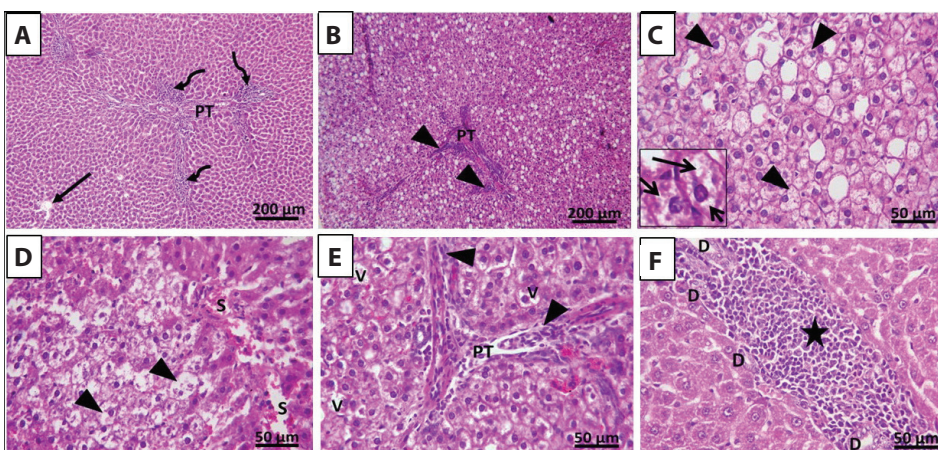

Figure 5. Photomicrographs of H&E stained liver sections from HFHF-OVX group. **A.** Classic hepatic lobules; central vein (↑), expanded portal tracts (PT) and cellular infiltrations (curved arrow) are seen. Notice bridging between portal tracts of adjacent lobules (×100). **B.** Expanded portal tract (PT) with mononuclear cellular infiltrations (▲). Vacuolations of hepatocytes are seen in all lobules (×100). **C.** Disturbed radial arrangement of hepatic cords and obliterated blood sinusoids. Ballooned hepatocytes (▲) are seen with peripheral nuclei. Inset: Mallory bodies (↑) are seen inside hepatocytes as eosinophilic intracytoplasmic structure (×400, inset ×1000). **D.** Dilated congested hepatic sinusoids (S). Some ballooned hepatocytes (▲) are seen with dark stained shrunken pyknotic nuclei and vacuolated cytoplasm (×400). **E.** Expanded portal tract (PT) with numerous inflammatory cells (▲). Vacuolated hepatocytes (V) are also seen (×400). **F.** Expanded portal tract with proliferated bile ducts (D) and cellular infiltration (*) (×400). For abbreviations, see Fig. 1.

Sham group (Fig. 8A). In OVX group, many small-sized red lipid droplets were seen in many hepatocytes (Fig. 8B). HFHF-OVX group showed increase in number and size of lipid droplets in most hepatocytes (Fig. 8C). On the other hand, rats in CeO$_2$-HFHF-OVX group showed occasional red lipid droplets in some hepatocytes (Fig. 8D).

Histomorphometric studies

Concerning the liver steatosis score and mean area% of Oil Red O stain for lipid droplets, they were significantly elevated in OVX rats *vs*. Sham group, and in HFHF-OVX group *vs*. Sham and OVX rats (Table 3). CeO$_2$-NPs treatment significantly decreased liver steatosis score in CeO$_2$-HFHF-OVX group in comparison to HFHF-OVX rats, though it was still significantly higher than the sham value. Furthermore, mean area% of Oil Red O stain for lipid droplets was significantly decreased in CeO$_2$-HFHF-OVX group *vs*. OVX and HFHF-OVX groups, achieving the sham value.

Regarding inflammation, Mallory-Denk bodies and ballooning scores, they were significantly increased in OVX and HFHF-OVX rats *vs*. Sham group (Table 2). Also, HFHF-OVX rats showed a significantly higher values of Mallory-Denk bodies and ballooning scores compared to OVX rats. All these changes were significantly alleviated in CeO$_2$-HFHF-OVX group vs. HFHF-OVX group, although only the Mallory-Denk bodies score approached the sham value.

Additionally, lobular fibrosis and portal fibrosis scores as well as mean area % of collagen fibers were significantly
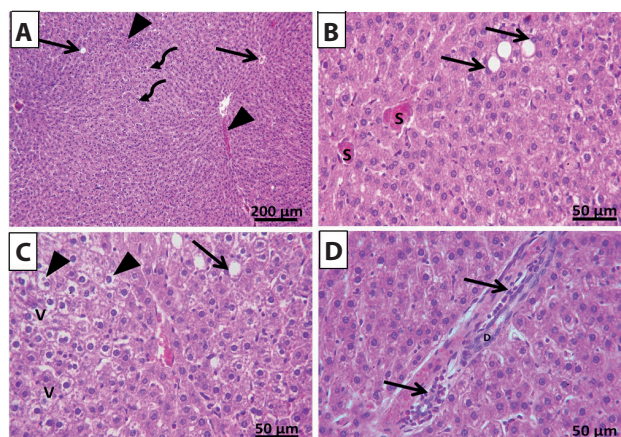

Figure 6. Photomicrographs of H&E stained liver sections from CeO$_2$-HFHF-OVX group. **A.** Central vein (↑) and peripheral portal tracts (▲). Focal area of vacuolated hepatocytes is seen (curved arrow) (×100). **B.** Few dilated congested hepatic sinusoids (S). Some hepatocytes are seen with intracellular vacuoles and peripheral nuclei (↑) (×400). **C.** Some hepatocytes are seen vacuolated (V), others are seen ballooned (▲). Hepatocytes with peripheral nucleus (↑) and intracellular vacuoles are seen (×400). **D.** Portal tract with bile duct branch (D). Few inflammatory cells (↑) are seen (×400). For abbreviations, see Fig. 1.

higher in OVX and HFHF-OVX groups compared to Sham group (Table 2). HFHF-OVX rats, also, showed a significantly elevated mean area % of collagen fibers in comparison to OVX group. All these values were significantly decreased by

Table 1. Serum levels of lipid profile, oxidative stress markers, and liver inflammatory markers in the different studied groups

	Sham	OVX	HFHF-OVX	CeO$_2$-HFHF-OVX
Lipid profile				
TG (mg/dl)	71.43 ± 1.83	104.41 ± 2.93[a]	114.01 ± 2.00[a,b]	90.56 ± 1.33[a,b,c]
TC (mg/dl)	122.34 ± 1.69	181.35 ± 2.55[a]	208.85 ± 3.44[a,b]	162.99 ± 3.79[a,b,c]
HDL-C (mg/dl)	59.43 ± 1.14	41.14 ± 1.65[a]	36.91 ± 1.44[a,b]	49.40 ± 1.26[a,b,c]
LDL-C (mg/dl)	48.62 ± 1.87	119.33 ± 3.08[a]	149.14 ± 3.42[a,b]	95.48 ± 3.72[a,b,c]
AI	0.08 ± 0.02	0.41 ± 0.03[a]	0.49 ± 0.02[a,b]	0.26 ± 0.01[a,b,c]
Oxidative markers				
MDA (nmol/ml)	29.04 ± 2.14	85.58 ± 4.17[a]	116.11 ± 2.20[a,b]	59.52 ± 2.28[a,b,c]
TAC (mmol/l)	57.54 ± 2.43	25.65 ± 1.82[a]	19.94 ± 1.29[a,b]	41.03 ± 1.23[a,b,c]
Inflammatory markers				
TNF-α (pg/g tissue)	60.21 ± 2.79	113.99 ± 3.25[a]	156.35 ± 6.13[a,b]	80.69 ± 2.96[a,b,c]
TGF-β1 (pg/g tissue)	31.52 ± 1.25	97.80 ± 2.85[a]	128.96 ± 3.64[a,b]	58.40 ± 3.99[a,b,c]

Values are presented as mean ± SEM. OVX, ovariectomized group; HFHF-OVX, high-fat high-fructose diet-fed OVX group; CeO$_2$-HFHF-OVX, HFHF-OVX cerium oxide-treated group; TG, triglycerides; TC, total cholesterol; HDL-C, high density lipoprotein cholesterol; LDL-C, low density lipoprotein cholesterol; AI, Atherogenic index; MDA, malondialdehyde; TAC, total antioxidant capacity; TNF-α, tumor necrosis factor alpha; TGF-β1, transforming growth factor beta-1. Inter-group significance was done by One way ANOVA and Fisher's least significant difference. [a] $p < 0.05$ *vs*. Sham group, [b] $p < 0.05$ *vs*. OVX group, [c] $p < 0.05$ *vs*. HFHF-OVX group.
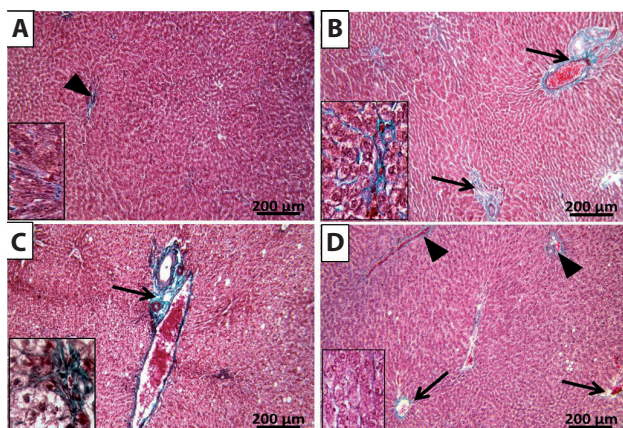
Figure 7. Photomicrographs of Masson`s trichrome stained liver sections from different studied groups. **A.** Sham group. Few collagen fibers in the portal tract (▲) and around central veins. Inset: minimal amounts of collagen fibers between hepatocytes (×100, inset ×400). **B.** OVX group. An increase amount of collagen fibers (↑) in some portal tracts. Inset: an increase amount of collagen fibers is seen between hepatocytes (×100, inset ×400). **C.** HFHF-OVX group. Increased collagen fibers (↑) in the expanded portal tract. Inset: an increase amount of collagen fibers is seen between hepatocytes (×100, inset ×400). **D.** CeO$_2$-HFHF-OVX group. Few collagen fibers (↑) around central vein and portal tracts (▲). Inset: minimal amount of collagen fibers is seen between hepatocytes (×100, inset ×400). For abbreviations, see Fig. 1.

CeO$_2$-NPs treatment in CeO$_2$-HFHF-OVX group *vs.* OVX and HFHF-OVX groups, however, only the portal fibrosis score attained the sham value.

Discussion

In the present study, we explored the ability of CeO$_2$-NPs to alleviate the NAFLD and NASH in postmenopausal obese rats and clarified the underlying mechanisms.

Ovariectomy, in the present study, significantly increased both overall and visceral obesity in OVX rats *vs.* Sham group. In concomitance, a significant increase in liver lipid accumulation, liver steatosis, liver inflammation, ballooned hepatocytes, Mallory-Denk bodies (the hall marks of liver steatohepatitis (Brown and Kleiner 2016)), and liver collagen fibers deposition, along with a significant elevation in liver enzymes, liver tissue levels of TNF-α and TGF-β1 were observed in OVX group compared to Sham group. These findings indicate that ovariectomy induced NAFLD and liver injury which progress to NASH with an apparent enhancement of inflammation and even liver fibrosis, which could be explained by the associated obesity. Moreover, as the overall obesity parameters increased by consumption of HFHF diet by OVX rats, the severity of liver injury, steatosis, inflammation as well as fibrosis were significantly enhanced in HFHF-OVX group *vs.* both Sham and OVX rats; confirming the crucial role of obesity in mediating such liver pathologies.

CeO$_2$-NPs treatment significantly attenuated both overall and visceral obesity in CeO$_2$-HFHF-OVX rats *vs.* both OVX and HFHF-OVX groups. In parallel, liver steatosis and steatohepatitis were significantly alleviated as demonstrated by the histological studies as well as the significantly lowered liver tissue levels of FFA, TNF-α and TGF-β1 in CeO$_2$-HFHF-OVX rats compared to HFHF-OVX group. These changes were appropriate to mitigate liver injury and liver fibrosis as manifested by the significant decrease in AST, ALT, mean area % of collagen fibers, and lobular and portal fibrosis in CeO$_2$-HFHF-OVX group *vs.* HFHF-OVX group. Such obvious hepatoprotective effect of cerium oxide could be induced via its ability to decrease obesity. The ameliorative effect of nanoceria against liver steatosis (Wasef et al. 2021) as well as obesity (Rocca et al. 2015) was previously demonstrated by experimental studies.

Obesity particularly with central fat deposition is a chief component that promotes the development of NAFLD (Vulf

Table 2. Histopathological scoring system in the different studied groups

	Sham	OVX	HFHF-OVX	CeO$_2$-HFHF-OVX
Steatosis[#]	0 (0–1)	1 (0–2)[a]	3 (0–3)[a,b]	0 (0–3)[a,c]
Inflammation[#]	0 (0–2)	2 (1–3)[a]	2 (0–3)[a]	0.5 (0–2)[a,b,c]
Mallory-Denk bodies[#]	0 (0–0)	0 (0–1)[a]	2 (0–2)[a,b]	0 (0–1)[c]
Ballooning[#]	0 (0–0)	0 (0–2)[a]	3 (0–3)[a,b]	1 (0–1)[a,c]
Lobular fibrosis[#]	0 (0–2)	2 (0–3)[a]	2 (0–3)[a]	0.5 (0–2)[a,b,c]
Portal fibrosis[#]	0 (0–2)	2 (0–3)[a]	2 (0–3)[a]	0 (0–2)[b,c]
Mean area % of Oil Red O stain for lipid droplets	0.96 ± 0.1	16.89 ± 0.9[a]	29.53 ± 0.8[a,b]	2.83 ± 0.3[b,c]
Mean area % of collagen fibers	2.07 ± 0.3	8.58 ± 0.4[a]	17.48 ± 0.3[a,b]	3.68 ± 0.2[a,b,c]

Data are mean ± SEM; [#] median (range); [a] $p < 0.05$ *vs.* Sham group; [b] $p < 0.05$ *vs.* OVX group; [c] $p < 0.05$ *vs.* HFHF-OVX group. For abbreviations, see Table 1.

et al. 2018). NAFLD was demonstrated in 70 to 80% of subjects with central obesity (Williamson et al. 2011). Obesity is triggered by estrogen loss in menopause and primarily drives the process of liver lipid infiltration (Kamada et al. 2011). Experimental studies have reported an increase in body weight and visceral fat after 6 weeks (Pighon et al. 2011) and 12 weeks (Jeong et al. 2018) of ovariectomy in rats and mice, respectively. Visceral fat, has a strong lipolytic activity that increases FFA flux to the liver, and promotes liver steatosis (Pedersen et al. 2004; Verrijken et al. 2011).

Also, increased consumption of energy-dense foods containing high amounts of fats and fructose represents another aggravating factor for obesity (Zivkovic et al. 2007). Estrada Cruz et al. (2019) stated that HFHF diet is a further promoter to weight gain in OVX animals. High fructose consumption has been associated with increased de novo lipogenesis, insulin resistance, and visceral adiposity (Ter Horst and Serlie 2017). Prevention of obesity was found to reduce fatty liver in high-fat fed mice (Kim et al. 2018). Thus, the ability of CeO$_2$-NPs to attenuate liver steatosis and its deleterious consequences in ovariectomized obese rats, in the present study, might be partly related to its anti-obesity effect, in particular visceral obesity.

Additionally, ovariectomy, in the current study, disrupted the lipid metabolism as indicated by the significant dyslipidemia together with the significant upregulation of liver LXR expression, and downregulation of liver SHP expression in OVX group *vs.* Sham group, all are strong mediators of liver lipid accumulation.

LXR is a key regulator of hepatic lipogenesis. Its lipogenic activity is mediated *via* upregulation of sterol regulatory element-binding protein-1c (SREBP-1c), acetyl-CoA carboxylase 1 (ACC1), and sterol-CoA desaturase 1 (SCD1); all leading to increased hepatic lipid levels, one of the etiological agents in the pathogenesis of NAFLD. Also, LXR stimulates the carbohydrate response element-binding protein (ChREBP) (Grønning-Wang et al. 2013) that increases the conversion of carbohydrates into lipids in liver.

Further, SHP, an orphan member of the nuclear hormone receptor superfamily, predominantly functions as a transcriptional repressor of gene expression by directly binding to a variety of nuclear receptors (Zhang et al. 2011). SHP decreases the expression of SREBP-1c, an important factor in regulating the lipogenic program in liver, as well as LXR (Watanabe et al. 2004; Zhang et al. 2011), denoting its anti-lipogenic effect.

Moreover, estrogen deficiency diverted the hepatic metabolism from lipid oxidation to fatty acid biosynthesis, thus favoring its esterification and accumulation as triacylglycerols in the cytosol of hepatocytes (Paquette et al. 2008). Estradiol was demonstrated to modulate hepatic lipogenesis by decreasing the levels of lipogenic genes, namely SREBP-1c, ACC1, and SCD1, and to prevent hepatic fat accumulation
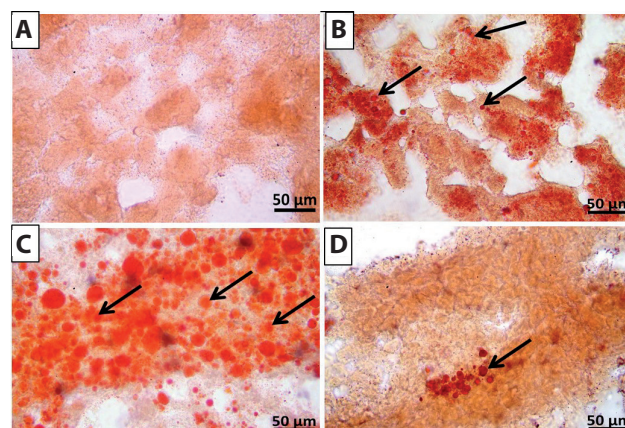

Figure 8. Photomicrographs of Oil Red O stained liver sections from different studied groups. **A.** Sham group. No red deposits in hepatocytes (×400). **B.** OVX group. Many small sized red lipid droplets (↑) in hepatocytes (×400). **C.** HFHF-OVX group. Increased number and size of red lipid droplets (↑) (×400). **D.** CeO$_2$-HFHF-OVX group. Few red lipid droplets (↑) (×400). For abbreviations, see Fig. 1.

in ovariectomized female rats (Pighon et al. 2011). Estrogen receptor ligands can reduce TG in the mouse liver by inhibiting LXR transcriptional activity (Han et al. 2014). Furthermore, hepatic estrogen receptor α activation can improve liver steatosis *via* upregulation of SHP (Wang et al. 2015).

Also, lacking of estrogen is associated with increased risk for many metabolic derangements including, dyslipidemia (Lovegrove et al. 2002). Several studies have highlighted the strong relationship between NAFLD and increased serum TG, small dense LDL and low HDL (Sung et al. 2012).

Table 3. Correlation coefficients evaluated from correlation studies of LXR (liver X receptor) and SHP (short heterodimer partner), with liver FFA (free fatty acid), serum lipid profile as well as histological scores

	LXR	SHP
FFA	0.917	−0.885
TG	0.865	−0.871
TC	0.918	−0.927
HDL	−0.801	0.787
LDL	0.911	−0.922
AI	0.898	−0.891
Steatosis	0.755	−0.719
Inflammation	0.754	−0.758
Mallory Bodies	0.741	−0.688
Ballooning	0.639	−0.589

In all correlations, $p = 0.000$ (a value of $p \leq 0.05$ is considered statistically significant). For abbreviations, see Table 1.

Dyslipidemia has been demonstrated in 20 to 80% of cases associated with NAFLD (Souza et al. 2012).

Additionally, HFHF diet, herein, significantly aggravated the dyslipidemia and increased liver LXR and decreased SHP mRNA expression in HFHF-OVX group compared to OVX group. Fructose is metabolized by the liver, where it activates hepatic de novo lipogenesis acting primarily *via* SREBP-1c and ChREBP, prevents the mitochondrial β-oxidation of long-chain fatty acids, causes endoplasmic reticulum stress, and enhances TG formation and hepatic steatosis (Lim et al. 2010; Softic et al. 2020).

According to the present results and the aforementioned reports, both ovariectomy and HFHF diet, in the present study, synergistically disturbed lipid metabolism *via* modulating the gene expression of lipogenic pathways in liver; increasing lipogenesis and inducing dyslipidemia, all enhance liver steatosis and steatohepatitis.

CeO_2-NPs treatment in the present study, significantly downregulated the LXR, lowered dyslipidemia and upregulated the SHP gene expression in liver tissues in CeO_2-HFHF-OVX rats *vs.* both OVX and HFHF-OVX groups. These results provide evidence that cerium oxide can diminish the disturbed lipid metabolism and dyslipidemia produced by ovariectomy and HFHF diet *via* readjusting the liver gene expression of both LXR and SHP. This postulate was further supported by the correlation studies.

To the best of our knowledge, the current study is the first to shed light on the ability of cerium oxide nanoparticles to modulate LXR and SHP gene expression in liver, which add to its anti-lipogenic effect. This effect could be a novel mechanism by which cerium oxide can attenuate liver steatosis and steatohepatitis. In agreement with this postulate, Wasef et al. (2021) have demonstrated that CeO_2 treatment can attenuate liver steatosis *via* decreasing dyslipidemia, downregulating the liver lipogenesis gene, ACC1, in a rat model of NAFLD. Also, Rocca et al. (2015) proved that six weeks of treatment with nanoceria produces a significant downregulation of the mRNA transcription of the main adipogenesis genes, namely a) glycerol-3-phosphate dehydrogenase 1, b) lipoprotein lipase, and c) lactate dehydrogenase A.

Also, OVX rats, in the present study, showed a significant increase in serum levels of MDA, along with a significant decrease in TAC *vs.* Sham group, reflecting increased oxidative stress in association with ovariectomy which could promote NAFLD and NASH. In support, the present significant increase in the severity of NAFLD and NASH was accompanied by a significantly augmented oxidative stress in HFHF-OVX group *vs.* Sham and OVX rats, proving the important role of oxidative stress in enhancing fatty liver.

Accumulating evidence implicates ROS as strong contributors to liver lipid accumulation and development of NAFLD as well as NASH (Paradies et al. 2014). Increased liver lipid accumulation and levels of FFA induced by estrogen with-drawal during menopause (Hart-Unger et al. 2017) impair mitochondrial oxidation (Ipsen et al. 2018) and increase peroxisomal β-oxidation (Moreno-Fernandez et al. 2018).

Furthermore, both oxidative stress and lipid accumulation induce hepatocellular damage which together with fat-derived factors mediate the activation of local inflammatory reaction, and hepatic stellate cells (Luedde and Schwabe 2011; Sharma et al. 2015) that enhance the recruitment of neutrophils, T-lymphocytes and macrophages (Kazankov et al. 2019). Such chronic pathological inflammation along with persistent oxidative stress disturb tissue homeostasis, enhancing hepatic steatosis, fibrosis, cirrhosis, and liver failure (Robinson et al. 2016).

Additionally, HFHF diet in rats was found to increase the activity of hepatic NADPH oxidase with a consequent overproduction of superoxide anions, reduction of hepatic content of glutathione, SOD and glutathione peroxidase in association with excessive lipid accumulation in livers (Feillet-Coudray et al. 2019). Therefore, oxidative stress with the eventual activation of the local hepatic inflammation, observed in HFHF-OVX group herein, could be explained by estrogen withdrawal and HFHF diet and could, in part, mediate NAFLD and NASH in this group. CeO_2-NPs treatment in the present study significantly attenuated oxidative stress (decreased MDA and increased TAC), and inflammation (decreased liver tissue TNF-α and histological markers of inflammation) processes in CeO_2-HFHF-OVX rats compared to both OVX and HFHF-OVX groups. These findings highlight the antioxidant, and anti-inflammatory activities of CeO_2-NPs as important mechanisms in attenuation of liver steatosis and steatohepatitis. This assumption is in accord with earlier studies (Oró et al. 2016; Ibrahim et al. 2018; Carvajal et al. 2019; Adebayo et al. 2020).

CeO_2-NPs, a powerful antioxidant and anti-inflammatory agents both *in vitro* and *in vivo* (Dhall and Self 2018), can scavenge ROS and nitric oxide radicals (Dowding et al. 2012) and exert a multi-enzyme mimetic activity, including SOD (Korsvik et al. 2007), catalase (Cafun et al. 2013), and peroxidase (Heckert et al. 2008). Because of this strong antioxidant activities, CeO_2-NPs were, recently, considered as a safe therapeutic agents in liver diseases (Casals et al. 2021). The ability of antioxidants to downregulate the adipogenesis genes *via* its inhibitory effect on ROS has been postulated by previous reports (Jeon et al. 2014; Rocca et al. 2015). Further, CeO_2-NPs protect HepG2 cells from cell-induced oxidative damage, reducing ROS generation and inflammatory gene expression as well as regulation of kinase-driven cell survival pathways (Carvajal et al. 2019).

An important observation in the present study is the ability of CeO_2-NPs to significantly alleviate the hepatic fibrosis as demonstrated by the significant decrease in liver TNF-α and TGF-β, key regulators of liver fibrosis (Tsuchida and Friedman 2017), as well as the significant decrease in lobular

fibrosis and portal fibrosis scores, and mean area % of collagen fibers in CeO$_2$-HFHF-OVX group *vs.* OVX and HFHF-OVX groups. Hepatic fibrosis is primarily initiated by hepatocyte injury, and sustained inflammation which trigger signaling cascades, influencing many cell types, as hepatocytes, Kupffer cells and sinusoidal endothelial cells; ultimately resulting in hepatic stellate cells (HSCs) activation and excessive extracellular matrix synthesis. TNF-α and TGF-β have crucial role in these signaling cascades (Tsuchida and Friedman 2017).

Activation of TGF-β produces differentiation of quiescent HSCs into myofibroblast in which TGF-β-dependent Smad-signaling pathways are stimulated to increase extracellular matrix formation (Dooley and ten Dijke 2012). TGF-β stimulation in hepatocytes results in hepatocyte death and lipid accumulation *via* Smad-signaling and ROS formation that facilitate the development of NASH (Yang et al. 2014). Blocking TGF-β/Smad pathway was found to decrease liver fibrosis as well as liver injury markers (Yuan et al. 2018). Recently, Boey et al. (2021) demonstrated that CeO$_2$-NPs were able to reduce hepatic fibrosis in the cultured hepatic stellate cell line LX2, through lowering oxidative stress and TGF-β-mediated signaling. Furthermore, TNF-α, a pivotal proinflammatory cytokine, has been known as one of the earliest participants in a variety of hepatic injuries (Tilg and Diehl 2000). It enhances HSC survival, hepatocyte death, and immune cell activation, which are associated with enhanced liver fibrosis (Yang and Seki 2015). Moreover, it can activate Kupffer cells, exacerbating NASH and liver fibrosis in mice (Tomita et al. 2006). Hence, CeO$_2$-NPs, herein, orchestrate crucial signals in the fibrotic pathway, decreasing liver fibrosis in postmenopausal obesity.

Of note, the hepatoprotective effect of cerium oxide, in the current work, is incomplete as the liver enzymes, dyslipidemia, oxidative stress and inflammatory markers, histological markers of liver steatosis, inflammation, and fibrosis, all were still significantly higher in CeO$_2$-HFHF-OVX rats *vs.* Sham group. A higher dose and/or longer duration may result in full correction.

Conclusion

CeO$_2$-NPs treatment can attenuate liver steatosis, steatohepatitis, and even fibrosis with amelioration of liver injury in a rat model of postmenopausal obesity. This hepatoprotective effect could be mediated, in part, *via* decreasing obesity, particularly visceral obesity, reducing dyslipidemia, and modulating the genes involved in the pathways of lipid metabolism (LXR and SHP), decreasing the lipogenesis. Also, the antioxidant effect of cerium oxide disrupts the feedback loop among oxidative stress, inflammatory and fibrotic processes and could be considered as a prospective therapeutic approach mitigating the NAFLD and NASH in postmenopausal obesity. Future human studies are recommended to prove the hepatoprotective effect of cerium oxide nanoparticles in human.

References

Adebayo OA, Akinloye O, Adaramoye OA (2020): Cerium oxide nanoparticles attenuate oxidative stress and inflammation in the liver of diethylnitrosamine-treated mice. Biol. Trace Elem. Res. **193,** 214-225
https://doi.org/10.1007/s12011-019-01696-5

Boey A, Leong SQ, Bhave S, Ho HK (2021): Cerium oxide nanoparticles alleviate hepatic fibrosis phenotypes in vitro. Int. J. Mol. Sci. **22,** 11777
https://doi.org/10.3390/ijms222111777

Brown GT, Kleiner DE (2016): Histopathology of nonalcoholic fatty liver disease and nonalcoholic steatohepatitis. Metabolism **65,** 1080-1086
https://doi.org/10.1016/j.metabol.2015.11.008

Brunt EM, Janney CG, Di Bisceglie AM, Neuschwander-Tetri BA, Bacon BR (1999): Nonalcoholic steatohepatitis: a proposal for grading and staging the histological lesions. Am. J. Gastroenterol. **94,** 2467-2474
https://doi.org/10.1111/j.1572-0241.1999.01377.x

Cafun JD, Kvashnina KO, Casals E, Puntes VF, Glatzel P (2013): Absence of Ce3+ sites in chemically active colloidal ceria nanoparticles. ACS Nano **7,** 10726-10732
https://doi.org/10.1021/nn403542p

Carvajal S, Perramón M, Oró D, Casals E, Fernández-Varo G, Casals G, Parra M, González de la Presa B, Ribera J, Pastor Ó, et al. (2019): Cerium oxide nanoparticles display antilipogenic effect in rats with non-alcoholic fatty liver disease. Sci. Rep. **9,** 1-20
https://doi.org/10.1038/s41598-019-49262-2

Casals E, Zeng M, Parra-Robert M, Fernández-Varo G, Morales-Ruiz M, Jiménez W, Puntes V, Casals G (2020): Cerium oxide nanoparticles: advances in biodistribution, toxicity, and preclinical exploration. Small **16,** e1907322
https://doi.org/10.1002/smll.201907322

Casals G, Perramón M, Casals E, Portolés I, Fernández-Varo G, Morales-Ruiz M, Puntes V, Jiménez W (2021): Cerium oxide nanoparticles: A new therapeutic tool in liver diseases. Antioxidants **10,** 1-23
https://doi.org/10.3390/antiox10050660

Chalasani N, Younossi Z, Lavine JE, Charlton M, Cusi K, Rinella M, Harrison SA, Brunt EM, Sanyal AJ (2018): The diagnosis and management of nonalcoholic fatty liver disease: Practice guidance from the American Association for the Study of Liver Diseases. Hepatology **67,** 328-357
https://doi.org/10.1002/hep.29367

Charbgoo F, Bin Ahmad M, Darroudi M (2017): Cerium oxide nanoparticles: green synthesis and biological applications. Int. J. Nanomedicine **12,** 1401-1413
https://doi.org/10.2147/IJN.S124855

Córdoba-Jover B, Arce-Cerezo A, Ribera J, Pauta M, Oró D, Casals G, Fernández-Varo G, Casals E, Puntes V, Jiménez W, Morales-Ruiz M (2019): Cerium oxide nanoparticles improve liver regeneration after acetaminophen-induced liver injury and partial hepatectomy in rats. J. Nanobiotechnology **17,** 1-12
https://doi.org/10.1186/s12951-019-0544-5

DeCoteau W, Heckman KL, Estevez AY, Reed KJ, Costanzo W, Sandford D, Studlack P, Clauss J, Nichols E, Lipps J, et al. (2016): Cerium oxide nanoparticles with antioxidant properties ameliorate strength and prolong life in mouse model of amyotrophic lateral sclerosis. Nanomedicine **12,** 2311-2320
https://doi.org/10.1016/j.nano.2016.06.009

Dhall A, Self W (2018): Cerium oxide nanoparticles: a brief review of their synthesis methods and biomedical applications. Antioxidants (Basel) **7,** 97
https://doi.org/10.3390/antiox7080097

Dooley S, ten Dijke P (2012): TGF-β in progression of liver disease. Cell Tissue Res. **347,** 245-256
https://doi.org/10.1007/s00441-011-1246-y

Dowding JM, Dosani T, Kumar A, Seal S, Self WT (2012): Cerium oxide nanoparticles scavenge nitric oxide radical (˙NO). Chem. Commun. (Camb.) **48,** 4896-4898
https://doi.org/10.1039/c2cc30485f

Estrada Cruz NA, Almanza Pérez JC, Fortis Barrera Á, Gallardo JM, Manuel Apolinar L, Segura Uribe JJ, Orozco Suárez S, Coyoy Salgado A, Guerra Araiza C (2019): Acute administration of tibolone prevents oxidative stress in ovariectomized rats fed high-fat-and-fructose diet. Exp. Clin. Endocrinol. Diabetes **127,** 396-404
https://doi.org/10.1055/a-0659-9928

Feillet-Coudray C, Fouret G, Vigor C, Bonafos B, Jover B, Blachnio-Zabielska A, Rieusset J, Casas F, Gaillet S, Landrier JF, et al. (2019): Long-term measures of dyslipidemia, inflammation, and oxidative stress in rats fed a high-fat/high-fructose diet. Lipids **54,** 81-97
https://doi.org/10.1002/lipd.12128

Friedewald WT, Levy RI, Fredrickson DS (1972): Estimation of the concentration of low-density lipoprotein cholesterol in plasma, without use of the preparative ultracentrifuge. Clin. Chem. **18,** 499-502
https://doi.org/10.1093/clinchem/18.6.499

Grønning-Wang LM, Bindesbøll C, Nebb HI (2013): The role of liver – in hepatic de novo lipogenesis and cross-talk with insulin and glucose signaling. Lipid Metab. **2013,** 61-90

Han SI, Komatsu Y, Murayama A, Steffensen KR, Nakagawa Y, Nakajima Y, Suzuki M, Oie S, Parini P, Vedin LL, et al. (2014): Estrogen receptor ligands ameliorate fatty liver through a non-classical estrogen receptor/liver X receptor pathway in mice. Hepatology **59,** 1791-1802
https://doi.org/10.1002/hep.26951

Hart-Unger S, Arao Y, Hamilton KJ, Lierz SL, Malarkey DE, Hewitt SC, Freemark M, Korach KS (2017): Hormone signaling and fatty liver in females: analysis of estrogen receptor α mutant mice. Int. J. Obes. (Lond.) **41,** 945-954
https://doi.org/10.1038/ijo.2017.50

Heckert EG, Seal S, Self WT (2008): Fenton-like reaction catalyzed by the rare earth inner transition metal cerium. Environ. Sci. Technol. **42,** 5014-5019
https://doi.org/10.1021/es8001508

Hirst SM, Karakoti AS, Tyler RD, Sriranganathan N, Seal S, Reilly CM (2009): Anti-inflammatory properties of cerium oxide nanoparticles. Small **5,** 2848-2856
https://doi.org/10.1002/smll.200901048

Ibrahim HG, Attia N, Hashem FEZA, El Heneidy MAR (2018): Cerium oxide nanoparticles: In pursuit of liver protection against doxorubicin-induced injury in rats. Biomed. Pharmacother. **103,** 773-781
https://doi.org/10.1016/j.biopha.2018.04.075

Ipsen DH, Lykkesfeldt J, Tveden-Nyborg P (2018): Molecular mechanisms of hepatic lipid accumulation in non-alcoholic fatty liver disease. Cell. Mol. Life Sci. **75,** 3313-3327
https://doi.org/10.1007/s00018-018-2860-6

Jeon HJ, Seo MJ, Choi HS, Lee OH, Lee BY (2014): Gelidium elegans, an edible red seaweed, and hesperidin inhibit lipid accumulation and production of reactive oxygen species and reactive nitrogen species in 3T3-L1 and RAW264.7 cells. Phytother. Res. **28,** 1701-1709
https://doi.org/10.1002/ptr.5186

Jeong YH, Hur HJ, Jeon EJ, Park SJ, Hwang JT, Lee AS, Lee KW, Sung MJ (2018): Honokiol improves liver steatosis in ovariectomized mice. Molecules **23,** 1-8
https://doi.org/10.3390/molecules23010194

Kamada Y, Kiso S, Yoshida Y, Chatani N, Kizu T, Hamano M, Tsubakio M, Takemura T, Ezaki H, Hayashi N, Takehara T (2011): Estrogen deficiency worsens steatohepatitis in mice fed high-fat and high-cholesterol diet. Am. J. Physiol. Gastrointest. Liver Physiol. **301,** G1031-1043
https://doi.org/10.1152/ajpgi.00211.2011

Kazankov K, Jørgensen SMD, Thomsen K.L, Møller HJ, Vilstrup H, George J, Schuppan D, Grønbæk H (2019): The role of macrophages in nonalcoholic fatty liver disease and nonalcoholic steatohepatitis. Nat. Rev. Gastroenterol. Hepatol. **16,** 145-159
https://doi.org/10.1038/s41575-018-0082-x

Khajuria DK, Razdan R, Mahapatra DR (2012): Description of a new method of ovariectomy in female rats. Rev. Bras. Reumatol. **52,** 462-470
https://doi.org/10.1590/S0482-50042012000300016

Kim JW, Lee YS, Seol DJ, Cho IJ, Ku SK, Choi JS, Lee HJ (2018): Anti-obesity and fatty liver-preventing activities of Lonicera caerulea in high-fat diet-fed mice. Int. J. Mol. Med. **42,** 3047-3064
https://doi.org/10.3892/ijmm.2018.3879

Kleiner DE, Brunt EM, Van Natta M, Behling C, Contos MJ, Cummings OW, Ferrell LD, Liu YC, Torbenson MS, Unalp-Arida A, et al. (2005): Design and validation of a histological scoring system for nonalcoholic fatty liver disease. Hepatology **41,** 1313-1321
https://doi.org/10.1002/hep.20701

Korsvik C, Patil S, Seal S, Self WT (2007): Superoxide dismutase mimetic properties exhibited by vacancy engineered ceria nanoparticles. Chem. Commun. (Camb.) **10,** 1056-1058
https://doi.org/10.1039/b615134e

Lim, JS, Mietus-Snyder M, Valente A, Schwarz JM, Lustig RH (2010): The role of fructose in the pathogenesis of NAFLD and the metabolic syndrome. Nat. Rev. Gastroenterol. Hepatol. **7,** 251-264
https://doi.org/10.1038/nrgastro.2010.41

Lobo RA (2017): Hormone-replacement therapy: current thinking. Nat. Rev. Endocrinol. **13,** 220-231
https://doi.org/10.1038/nrendo.2016.164

Lovegrove JA, Silva KDRR, Wright JW, Williams CM (2002): Adiposity, insulin and lipid metabolism in post-menopausal women. Int. J. Obes. Relat. Metab. Disord. **26,** 475-486
https://doi.org/10.1038/sj.ijo.0801963

Luedde T, Schwabe RF (2011): NF-κB in the liver--linking injury, fibrosis and hepatocellular carcinoma. Nat. Rev. Gastroenterol. Hepatol. **8,** 108-118
https://doi.org/10.1038/nrgastro.2010.213

Manne NDPK, Arvapalli R, Graffeo VA, Bandarupalli VVK, Shokuhfar T, Patel S, Rice KM, Ginjupalli GK, Blough ER (2017): Prophylactic treatment with cerium oxide nanoparticles attenuate hepatic ischemia reperfusion injury in sprague dawley rats. Cell. Physiol. Biochem. **42,** 1837-1846
https://doi.org/10.1159/000479540

Manne V, Handa P, Kowdley KV (2018): Pathophysiology of nonalcoholic fatty liver disease/nonalcoholic steatohepatitis. Clin. Liver Dis. **22,** 23-37
https://doi.org/10.1016/j.cld.2017.08.007

Moreno-Fernandez ME, Giles DA, Stankiewicz TE, Sheridan R, Karns R, Cappelletti M, Lampe K, Mukherjee R, Sina C, Sallese A, et al. (2018): Peroxisomal β-oxidation regulates whole body metabolism, inflammatory vigor, and pathogenesis of nonalcoholic fatty liver disease. JCI Insight **3,** e93626
https://doi.org/10.1172/jci.insight.93626

Nassar SZ, Hassaan PS, Abdelmonsif DA, ElAchy SN (2018): Cardioprotective effect of cerium oxide nanoparticles in monocrotaline rat model of pulmonary hypertension: A possible implication of endothelin-1. Life Sci. **201,** 89-101
https://doi.org/10.1016/j.lfs.2018.03.045

Ni D, Wei H, Chen W, Bao Q, Rosenkrans ZT, Barnhart TE, Ferreira CA, Wang Y, Yao H, Sun T, et al. (2019): Ceria nanoparticles meet hepatic ischemia-reperfusion injury: the perfect imperfection. Adv. Mater. **31,** e1902956
https://doi.org/10.1002/adma.201902956

Onat A, Can G, Kaya H, Hergenç G (2010): „Atherogenic index of plasma" (log10 triglyceride/high-density lipoprotein-cholesterol) predicts high blood pressure, diabetes, and vascular events. J. Clin. Lipidol. **4,** 89-98
https://doi.org/10.1016/j.jacl.2010.02.005

Oró D, Yudina T, Fernández-Varo G, Casals E, Reichenbach V, Casals G, De La Presa BG, Sandalinas S, Carvajal S, Puntes V, Jiménez W (2016): Cerium oxide nanoparticles reduce steatosis, portal hypertension and display anti-inflammatory properties in rats with liver fibrosis. J. Hepatol. **64,** 691-698
https://doi.org/10.1016/j.jhep.2015.10.020

Palmisano BT, Zhu L, Stafford JM (2017): Role of estrogens in the regulation of liver lipid metabolism. Adv. Exp. Med. Biol. **1043,** 227-256
https://doi.org/10.1007/978-3-319-70178-3_12

Paquette A, Wang D, Jankowski M, Gutkowska J, Lavoie JM (2008): Effects of ovariectomy on PPAR alpha, SREBP-1c, and SCD-1 gene expression in the rat liver. Menopause **15,** 1169-1175
https://doi.org/10.1097/gme.0b013e31817b8159

Paradies G, Paradies V, Ruggiero FM, Petrosillo G (2014): Oxidative stress, cardiolipin and mitochondrial dysfunction in nonalcoholic fatty liver disease. World J. Gastroenterol. **20,** 14205-14218
https://doi.org/10.3748/wjg.v20.i39.14205

Pedersen SB, Kristensen K, Hermann PA, Katzenellenbogen JA, Richelsen B (2004): Estrogen controls lipolysis by up-regulating alpha2A-adrenergic receptors directly in human adipose tissue through the estrogen receptor alpha. Implications for the female fat distribution. J. Clin. Endocrinol. Metab. **89,** 1869-1878
https://doi.org/10.1210/jc.2003-031327

Pighon A, Gutkowska J, Jankowski M, Rabasa-Lhoret R, Lavoie JM (2011): Exercise training in ovariectomized rats stimulates estrogenic-like effects on expression of genes involved in lipid accumulation and subclinical inflammation in liver. Metabolism **60,** 629-639
https://doi.org/10.1016/j.metabol.2010.06.012

Robinson MW, Harmon C, O'Farrelly C (2016): Liver immunology and its role in inflammation and homeostasis. Cell. Mol. Immunol. **13,** 267-276
https://doi.org/10.1038/cmi.2016.3

Rocca A, Moscato S, Ronca F, Nitti S, Mattoli V, Giorgi M, Ciofani G (2015): Pilot in vivo investigation of cerium oxide nanoparticles as a novel anti-obesity pharmaceutical formulation. Nanomedicine **11,** 1725-1734
https://doi.org/10.1016/j.nano.2015.05.001

Sharma M, Mitnala S, Vishnubhotla RK, Mukherjee R, Reddy DN, Rao PN (2015): The riddle of nonalcoholic fatty liver disease: progression from nonalcoholic fatty liver to nonalcoholic steatohepatitis. J. Clin. Exp. Hepatol. **5,** 147-158
https://doi.org/10.1016/j.jceh.2015.02.002

Softic S, Stanhope KL, Boucher J, Divanovic S, Lanaspa MA, Johnson RJ, Kahn CR (2020): Fructose and hepatic insulin resistance. Crit. Rev. Clin. Lab. Sci. **57,** 308-322
https://doi.org/10.1080/10408363.2019.1711360

Souza MR, Diniz MFF, de Medeiros-Filho JEM, de Araújo MST (2012): Metabolic syndrome and risk factors for non-alcoholic fatty liver disease. Arq. Gastroenterol. **49,** 89-96
https://doi.org/10.1590/S0004-28032012000100015

Sung KC, Wild SH, Kwag HJ, Byrne CD (2012): Fatty liver, insulin resistance, and features of metabolic syndrome: relationships with coronary artery calcium in 10,153 people. Diabetes Care **35,** 2359-2364
https://doi.org/10.2337/dc12-0515

Tandra, S, Yeh MM, Brunt EM, Vuppalanchi R, Cummings OW, Ünalp-Arida A, Wilson LA, Chalasani N (2011): Presence and

significance of microvesicular steatosis in nonalcoholic fatty liver disease. J. Hepatol. **55,** 654-659
https://doi.org/10.1016/j.jhep.2010.11.021

Ter Horst KW, Serlie MJ (2017): Fructose consumption, lipogenesis, and non-alcoholic fatty liver disease. Nutrients **9,** 981
https://doi.org/10.3390/nu9090981

Tian Z, Li X, Ma Y, Chen T, Xu D, Wang B, Qu Y, Gao Y (2017): Quantitatively intrinsic biomimetic catalytic activity of nanocerias as radical scavengers and their ability against H(2)O(2) and doxorubicin-induced oxidative stress. ACS Appl. Mater. Interfaces **9,** 23342-23352
https://doi.org/10.1021/acsami.7b04761

Tilg H, Diehl AM (2000): Cytokines in alcoholic and nonalcoholic steatohepatitis. N. Engl. J. Med. **343,** 1467-1476
https://doi.org/10.1056/NEJM200011163432007

Tomita K, Tamiya G, Ando S, Ohsumi K, Chiyo T, Mizutani A, Kitamura N, Toda K, Kaneko T, Horie Y, et al. (2006): Tumour necrosis factor alpha signalling through activation of Kupffer cells plays an essential role in liver fibrosis of non-alcoholic steatohepatitis in mice. Gut **55,** 415-424
https://doi.org/10.1136/gut.2005.071118

Tsuchida T, Friedman SL (2017): Mechanisms of hepatic stellate cell activation. Nat. Rev. Gastroenterol. Hepatol. **14,** 397-411
https://doi.org/10.1038/nrgastro.2017.38

Verrijken AN, Francque S, Van Gaal L (2011): The role of visceral adipose tissue in the pathogenesis of non-alcoholic fatty liver disease. Eur. Endocrinol. **7,** 96-103
https://doi.org/10.17925/EE.2011.07.02.96

Vulf MA, Kirienkova EV, Skuratovskaia DA, Levada EV, Volkova LV, Zatolokin PA, Gazatova ND, Litvinova LS (2018): Factors governing development of nonalcoholic fatty liver disease and insulin resistance in obesity. Biomed. Khim. **64,** 444-450
https://doi.org/10.18097/PBMC20186405444

Wang X, Lu Y, Wang E, Zhang Z, Xiong X, Zhang H, Lu J, Zheng S, Yang J, Xia X, et al. (2015): Hepatic estrogen receptor α improves hepatosteatosis through upregulation of small heterodimer partner. J. Hepatol. **63,** 183-190
https://doi.org/10.1016/j.jhep.2015.02.029

Wasef L, Nassar AMK, El-Sayed YS, Samak D, Noreldin A, Elshony N, Saleh H, Elewa YHA, Hassan SMA, Saati AA, et al. (2021): The potential ameliorative impacts of cerium oxide nanoparticles against fipronil-induced hepatic steatosis. Sci. Rep. **11,** 1310
https://doi.org/10.1038/s41598-020-79479-5

Watanabe M, Houten SM, Wang L, Moschetta A, Mangelsdorf DJ, Heyman RA, Moore DD, Auwerx J (2004): Bile acids lower triglyceride levels via a pathway involving FXR, SHP, and SREBP-1c. J. Clin. Invest. **113,** 1408-1418
https://doi.org/10.1172/JCI21025

Williamson RM, Price JF, Glancy S, Perry E, Nee LD, Hayes PC, Frier BM, Van Look LAF, Johnston GI, Reynolds RM, Strachan MWJ (2011): Prevalence of and risk factors for hepatic steatosis and nonalcoholic fatty liver disease in people with type 2 diabetes: The Edinburgh type 2 diabetes study. Diabetes Care **34,** 1139-1144
https://doi.org/10.2337/dc10-2229

Yang L, Roh YS, Song J, Zhang B, Liu C, Loomba R, Seki E (2014): Transforming growth factor beta signaling in hepatocytes participates in steatohepatitis through regulation of cell death and lipid metabolism in mice. Hepatology **59,** 483-495
https://doi.org/10.1002/hep.26698

Yang YM, Seki E (2015): TNFα in liver fibrosis. Curr. Pathobiol. Rep. **3,** 253-261
https://doi.org/10.1007/s40139-015-0093-z

Yuan X, Gong Z, Wang B, Guo X, Yang L, Li D, Zhang Y (2018): Astragaloside inhibits hepatic fibrosis by modulation of tgf-β1/smad signaling pathway. Evid. Based Complement. Alternat. Med. **2018,** 3231647
https://doi.org/10.1155/2018/3231647

Zhang Y, Hagedorn CH, Wang L (2011): Role of nuclear receptor SHP in metabolism and cancer. Biochim. Biophys. Acta **1812,** 893-908
https://doi.org/10.1016/j.bbadis.2010.10.006

Zivkovic AM, German JB, Sanyal AJ (2007): Comparative review of diets for the metabolic syndrome: implications for nonalcoholic fatty liver disease. Am. J. Clin. Nutr. **86,** 285-300
https://doi.org/10.1093/ajcn.86.2.285